ARTICLES

Journal of Semiconductors
(2023) 44, 032701
doi: 10.1088/1674-4926/44/3/032701

A binder-free CF|PANI composite electrode with excellent capacitance for asymmetric supercapacitors

Kexin Li, Gentian Yue†, and Furui Tan†

Henan Key Laboratory of Photovoltaic Materials and Laboratory of Low-Dimensional Materials Science, Henan University, Kaifeng 475004, China

Abstract: In this work, carbon fiber and polyaniline (CF|PANI) composites are prepared by using an electrochemical polymerization method. The morphology and composition characterization results show that the PANI nanospheres are successfully synthesized and uniformly coated on the CF. When the electrodeposition period is 300 cycles, the as-prepared CF|PANI electrode exhibits good specific capacitance of 231.63 F/g at 1 A/g, high performance of 98.14% retention rate from 0.5 to 20 A/g, and excellent cycle stability with only 0.96% capacity loss after 1000 cycles. This is ascribed to the internal resistance that was significantly reduced without binders, which helps to the CF|PANI electrode maintains high operating potential and pseudo-capacitance performance at high current density. The symmetrical supercapacitor based on two CF|PANI electrodes connecting by acidic PVA-H_2SO_4 gel electrolyte exhibits an energy density of 6.55 W·h/kg at a power density of 564.37 W/kg. In addition, the asymmetric supercapacitor based on MoS_2|MWCNTs and CF|PANI electrodes with neutral PVA-Na_2SO_4 gel electrolyte shows an energy density of 16.12 W·h/kg at a power density of 525.03 W/kg. These results indicate that the low internal resistance contributes to the high energy density of symmetrical supercapacitors and asymmetric supercapacitors at high current density and high power density, which is significant for its practical application.

Key words: quasi-solid state supercapacitor; carbon fibers; binder-free; polyaniline

Citation: K X Li, G T Yue, and F R Tan, A binder-free CF|PANI composite electrode with excellent capacitance for asymmetric supercapacitors[J]. *J. Semicond.*, 2023, 44(3), 032701. https://doi.org/10.1088/1674-4926/44/3/032701

1. Introduction

Flexible quasi-solid state supercapacitors are widely considered to be an important clean and sustainable energy storage device. When used in an integrated photovoltaic energy storage system or grid transfer station, they are known for their light weight, portability, superior power density and long-term cycle stability[1–7]. In theory, the design of flexible supercapacitors can be achieved by vertically superimposing on quasi-solid electrolytes or horizontally depositing electrodes next to adjacent electrodes on flexible substrates[8–13]. Between two, the latter design is more conducive to the miniaturization of supercapacitors[14].

The polyaniline (PANI) is considered to be the most potential conductive polymer for supercapacitors thanks to its large theoretical pseudo-capacitance, high electrical conductivity, and low-cost. However, the stability of the main chain is poor because the swollen PANI shrinks during the doping/degumming process, which may lead to mechanical degradation, electrode ion and electrochemical decay, thus its wide application in portable devices and hybrid electric vehicles is limited[15–19]. To solve this problem, scientists have combined tantalum capacitor materials with well-stabilized carbon materials or transition metal compounds with special structures. Among them, carbon fiber (CF) as a typical electric double layer electrode material has been widely applied in flexible supercapacitors because of its flexibility and electrical conductivity. Wei *et al.*[20] fabricated the asymmetric device based on MXene//MnO_2 by chemical deposition and coating on CF, which exhibits specific capacitance of 20.5 F/g at 1.5 A/g, voltage window of 1.5 V more than twice wider than that of the symmetric device and energy density of 6.4 W·h/kg at power density of 1107.7 W/kg. Zhu *et al.*[21] prepared V_2O_5/CF composites with different mass ratios by a one-step hydrothermal method, whose specific capacity reaches 220.6 C/g at the current density of 1.0 A/g, and its capacitance retention is still 74.5% after 5000 incessant charge/discharge cycles. Seksar *et al.*[22] proposed to generate layered double hydroxide nanosheets (LDH NSs) from CF surface by hot-water therapy (HWT) method, and the Ni–Cu–Co LDH NSs/CF electrode demonstrated maximum areal capacity of 104.2 μA·h/cm^2 with an outstanding cycling stability of 124.5%. CF substrate exhibits excellent specific capacitance and stability performance after being loaded with tantalum capacitors such as MnO_2, V_2O_5 and LDH NSs, which can be used to make flexible supercapacitors without adhesives.

Molybdenum disulfide (MoS_2), as a typical transition metal compounds, has attracted considerable attention thanks to its special structural and chemical character, which is extensively applied in many fields including lithium-ion batteries, catalysis, and dye-sensitized solar cells. MoS_2 with nanoscale has recently been chosen for use in capacitors owing to its higher intrinsic fast ionic conductivity than oxides and higher theoretical capacity than graphite, as well as high surface area. Recently, many researchers have combined PANI with carbon materials and transition metal compound to im-

Correspondence to: G T Yue, yuegentian@126.com; F R Tan, frtan@henu.edu.cn
Received 3 SEPTEMBER 2022; Revised 18 SEPTEMBER 2022.

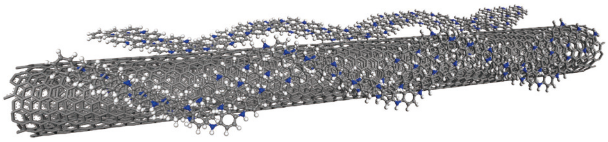

Fig. 1. The schematic diagram of the CF|PANI composite.

prove the conductivity of the PANI-based electrodes to enhance the cycling stability and rate capability of the PANI-based pseudo-super-capacitors[23–25]. Majumder *et al.*[26] combined CNOs with PANI by in situ oxidative polymerization of aniline monomer, which could significantly improve the overall electrochemical performance of PANI. Xu *et al.*[27] applied Co_3S_4/PANI obtained by introducing sulfur into ZIF-67/PANI to supercapacitors, where sulfur introduction can promote electron transfer with specific capacitance up to 11 times that of ZIF-67 at a current density of 1 A/g. Chen *et al.*[28] proposed using highly conductive graphene as a substrate to immobilize PANI in a hydrogel-based stretchable electrode. The electrode showed a high capacitance of 500.13 mF/cm^2 and 100% capacitance retention after 10 000 cycles of charge and discharge.

Inspired by these ideas, we activated the CF by using of electrochemical method, and then deposited the PANI nanoparticles on the surface to further prepare the CF|PANI composite electrode materials without adhesives. The specific capacitance of the CF|PANI composite electrode is 231.63 F/g at 1 A/g, and it still has 230.77 F/g (99.6% capacity retention), even at a current density of 20 A/g. Furthermore, the capacitance retention of the CF|PANI composite electrode is 99.04% after 1000 cycles. The prepared asymmetric super capacitor (ASC) based on the CF|PANI and MoS_2|MWCNT composite electrode and symmetric super capacitor (SSC) with two CF|PANI electrodes both exhibited good specific capacitance and energy density. Besides, two such ASC can easily light a LED lamp after being connected in series. These good electrochemical performance, long cycle stability, and excellent capacitive properties indicate that the CF|PANI composite materials have potential for application in portable energy storage equipment.

2. Experiment

2.1. Preparation of the CF|PANI composite electrode

The CF was first activated by using the cyclic voltammetry (CV) method for about 5 min at a scan rate of 50 mV/s between 1 and 2 V based on the previous reference[29]. Subsequently, it was stored in absolute ethanol. Then, 3.73 g aniline monomer was added to 80 mL 1 M H_2SO_4 solution. The activated CF was in situ electrochemically deposited PANI at a cycle rate of 100 mV/s from voltage windows of –0.2 to 0.8 V by meaning of a CV cycle. The obtained CF|PANI composite materials (Fig. 1) were washed 5 times or more with deionized water and absolute ethanol, and then vacuum dried at 50 °C for 24 h. The stability of the entire system was maintained at 50 °C during electrochemical deposition. The samples with the mass loading of 4.3, 6.4, 7.8, and 8.1 mg were labeled CF|PANI2, CF|PANI3, CF|PANI4, and CF|PANI5 under cycles of 200, 300, 400, and 500 cycles, respectively.

2.2. Preparation of quasi-solid SSC and ASC

The prepared CF|PANI electrode was first activated by 1 M KOH solution. Then, a gel electrolyte PVA-H_2SO_4 (or PVA-Na_2SO_4) was prepared, based on the previous reference[30, 31]. PVA (2 g) was dissolved in 20 mL deionized water under magnetically stirring at 90 °C until the solution became clear. Subsequently, it was uniformly mixed with 1 M H_2SO_4 (or Na_2SO_4) in a volume ratio of 1 : 1. The mixed solution was then subjected to an aging process to form the corresponding gel electrolyte. A quasi-solid SSC (CP3//CP3 SSC) was prepared by combining two CF|PANI3 electrodes and PVA-H_2SO_4 gel electrolyte. Moreover, the MoS_2|MWCNT (MM) electrodes were also prepared as in our published work[29]. A quasi-solid ASC (MM//CP3 ASC) was also prepared by combining the MoS_2|MWCNT and CF|PANI3 electrodes with PVA-H_2SO_4 gel electrolyte.

2.3. Characterization and electrochemical measurements

The surface morphologies of the samples were observed using a JSM-7001F field emission scanning electron microscope (SEM). Cyclic voltammetry (CV) measurements were conducted in a three-electrode one-compartment cell, in which an as-prepared sample electrode was taken as the working electrode, a Pt sheet of 1.5 cm^2 as CE and an Ag/AgCl electrode as reference electrode in 6 M aqueous KOH solution. The EIS tests were carried out simulating open-circuit conditions at ambient atmosphere by using an electrochemical measurement system (CHI660E, Shanghai Chenhua Device Company, China) at a constant temperature of 20 °C with AC signal amplitude of 20 mV in the frequency range from 0.1 to 10^5 Hz at 0 V DC bias in the dark. The galvanostatic current charge-discharge (GCD) curves were conducted by using a computer-controlled electrochemical analyzer (CHI 660E, CH Instrument). The specific capacitance (C_s), energy density (E) and power density (P) of the supercapacitor were calculated according to the following equations[32–35]:

$$C_s = \frac{I\Delta t}{m\Delta U} = \frac{Q}{m\Delta U}, \tag{1}$$

$$C_s = 4\frac{I\Delta t}{m_t\Delta U} = 4C_t, \tag{2}$$

$$E = \frac{C_t\Delta U^2}{7.2} \quad (\mathrm{W\cdot h/kg}), \tag{3}$$

$$P = \frac{3600E}{\Delta t} \quad (\mathrm{W/kg}), \tag{4}$$

where I represents the current density (A), Δt represents the discharge time (s), ΔU represents the working potential window (V), m represents the quality of active materials (g), Q refers to the amount of charge that can be stored, C_s represents the specific capacitance of the individual electrode, and C_t and m_t represent the specific capacitance of the supercapacitor and the total mass of the active material, respectively.

3. Results and discussion

Fig. 2(a) shows clearly that the color of the CF exhibited black color before pretreatment. After electrochemical pretreating, the color of the CF surface turned purple (Fig. 2(b)). Then, PANI was deposited on the pretreated CF surface, and

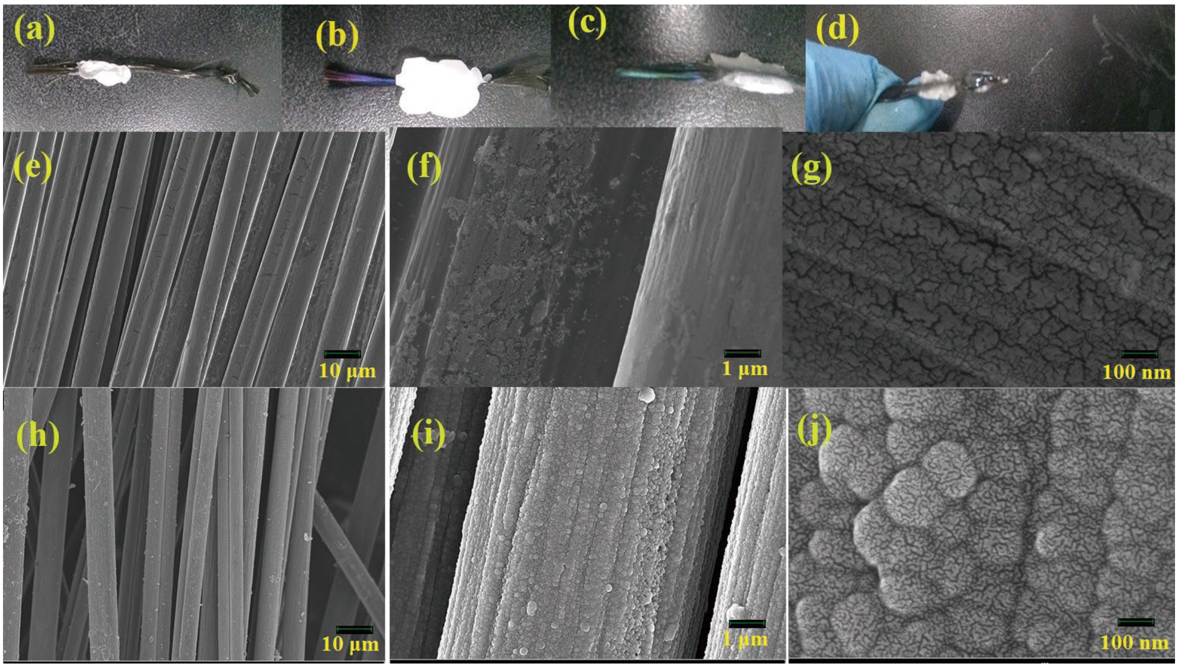

Fig. 2. (Color online) Optical diagram of (a) the CF, (b) CF after electrochemical activation, (c) the CF|PANI3, (d) the CF|PANI3 overcoated with PVA-H_2SO_4. SEM images of the pretreated CF bundle at (e) 1000, (f) 10 000 and (g) 100 000 magnification; the SEM images of pretreated CF|PANI3 at (h) 1000, (i) 10 000 and (j) 100 000 magnification.

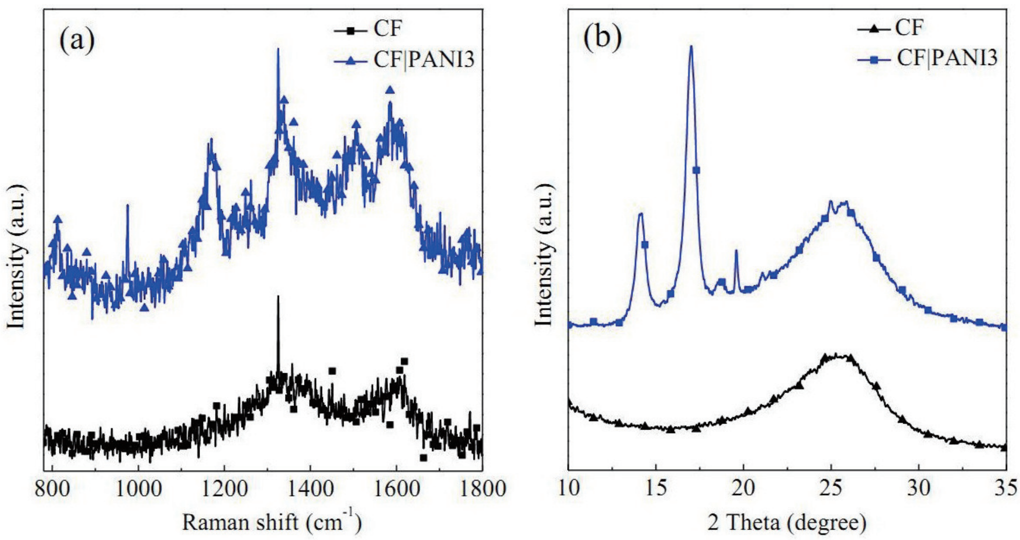

Fig. 3. (Color online) (a) Raman spectrum and (b) XRD spectrum of CF|PANI3.

the green CF|PANI composite was obtained as shown in Fig. 2(c). After electrochemical deposition and annealing treatment, the PVA-H_2SO_4 electrolyte was loaded onto the CF|PANI3 surface, as shown in Fig. 2(d). Figs. 2(e)–2(g) present the SEM images of the pretreated CF at 1000, 10 000, and 100 000 magnifications, respectively. As the amplification factor increased, the surface voids of the CF gradually appeared, which is helpful for the active substances loading on CF bundle. Figs. 2(h)–2(j) are SEM images of CF|PANI3 electrode at 1000, 10 000, and 100 000 magnifications, respectively. Among them, PANI nanoparticles are well loaded on the surface of the CF bundles. At a magnification of 100 000, it can be seen that the PANI on CF surface has more wrinkles, which greatly promotes the improvement of their specific surface area.

Fig. 3(a) shows the Raman spectrum of CF and CF|PANI3. From Fig. 3(a), the characteristic peaks of CF are close to the D and G bands of graphite material, which are near 1350 and 1580 cm^{-1}, respectively. The intensity ratio of D/G (about 1) and the density of defects are relatively large[36], which is responsible for the pretreatment of CF. This is very advantageous for the active material PANI to be loaded thereon. The Raman characteristic peaks of the CF|PANI3 are all appear at 1161, 1255, 1346, 1481, and 1583 cm^{-1}[29]. Among them, the peak near 1583 cm^{-1} is caused by the benzene ring type tensile vibration and the C–C type of the polymer type; the peak near 1481 cm^{-1} is strengthened, and each band has a high/low wave number in the aniline salt spectrum[37]. At the Raman spectrum of CF|PANI3, the characteristic peaks of CF are faintly visible. This result indicates that the nanoscale PANI has covered the CF surface very well.

Fig. 3(b) shows the XRD spectrum of the CF and

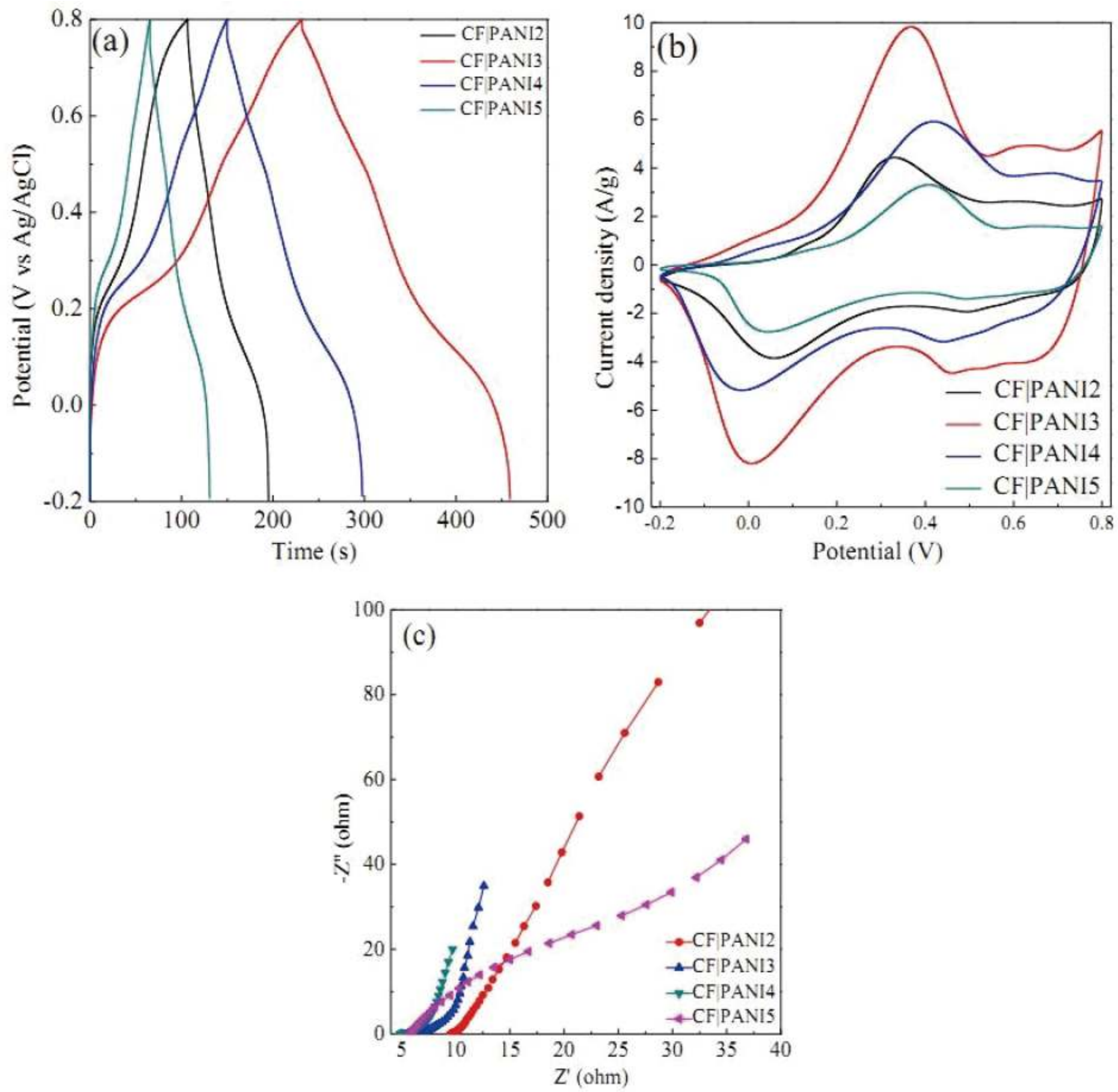

Fig. 4. (Color online) (a) GCD curves of the different electrodes at 1 A/g condition. (b) CVs for the different electrodes at 20 mV/s condition. (c) EIS for the different electrodes.

CF|PANI3. Among them, the broad peak at 24° ((002) crystal plane) represents graphite carbon[31, 38]. The XRD characteristic peaks of pure PANI are about 15.1° (011), 20.5° (020), and 25.5° (200)[39]. The appearance of the XRD peaks in the middle is due to the diffraction of the layered polymer on the alternating distance and semi-crystalline surface of polyaniline[40].

From Fig. 4(a), it can be seen that the discharge time of the various CF|PANI composite electrodes increases at first and then decreases as the electrodeposition period increases. From Eq. (1), the corresponding specific capacitances for the above CF|PANI composite electrodes also increase at first and then decrease from. When the electrodeposition period is 300 cycles, the specific capacitance of CF|PANI3 is the largest. Fig. 4(b) shows the CVs of the various electrodes under 20 mV/s condition, in which the redox peaks of the different electrodes increase firstly and then decrease with the electrodeposition cycle increasing. Among them, the redox peak of the CF|PANI3 electrode exhibits most obviously, indicating its good pseudo-capacitance. At the same scanning speed, the area enclosed by the CV of the CF|PANI3 electrode is the largest, and thus the specific capacitance is also the largest according to Eq. (2). This result is consistent with the previous calculation of constant current charge and discharge.

Fig. 4(c) shows the EIS of the various electrodes with different deposition cycles. From Fig. 4(c), it can be seen that the internal resistance (R_s: high frequency region, the first intersection of the impedance line and the real axis) of the CF|PANI composite electrodes decreases as the electrodeposition period increases. Among them, the slope of the CF|PANI3 electrode in the low frequency region is the smallest, indicating its best ion diffusion and conductivity ability[41]. Moreover, the lower equivalent series internal resistance and charge transfer internal resistance (R_{ct}: high frequency region to intermediate frequency region, the diameter of the impedance circle is semicircular) for the CF|PANI3 electrode compared to other electrodes indicates that CF|PANI3 electrode possesses better rate performance.

Table 1 shows the specific capacity (C_s) and voltage drop (U_{drop}) of the CP|PANI2, CP|PANI3, CP|PANI4, and CP|PANI5 electrode at 1 A/g condition. Among these electrodes, the specific capacitance of the CP|PANI3 electrode can reach 231.63 F/g, which is much larger than that of the CF|PANI2

Table 1. The U_{drop} and C_s values of the CF|PANI2, CF|PANI3, CF|PANI4, and CF|PANI5 electrodes at 1 A/g condition.

Composite electrode	CF|PANI2	CF|PANI3	CF|PANI4	CF|PANI5
U_{drop} (V)	0.01	0.02	0.04	0.06
C_s (F/g)	97.98	231.63	153.65	70.21

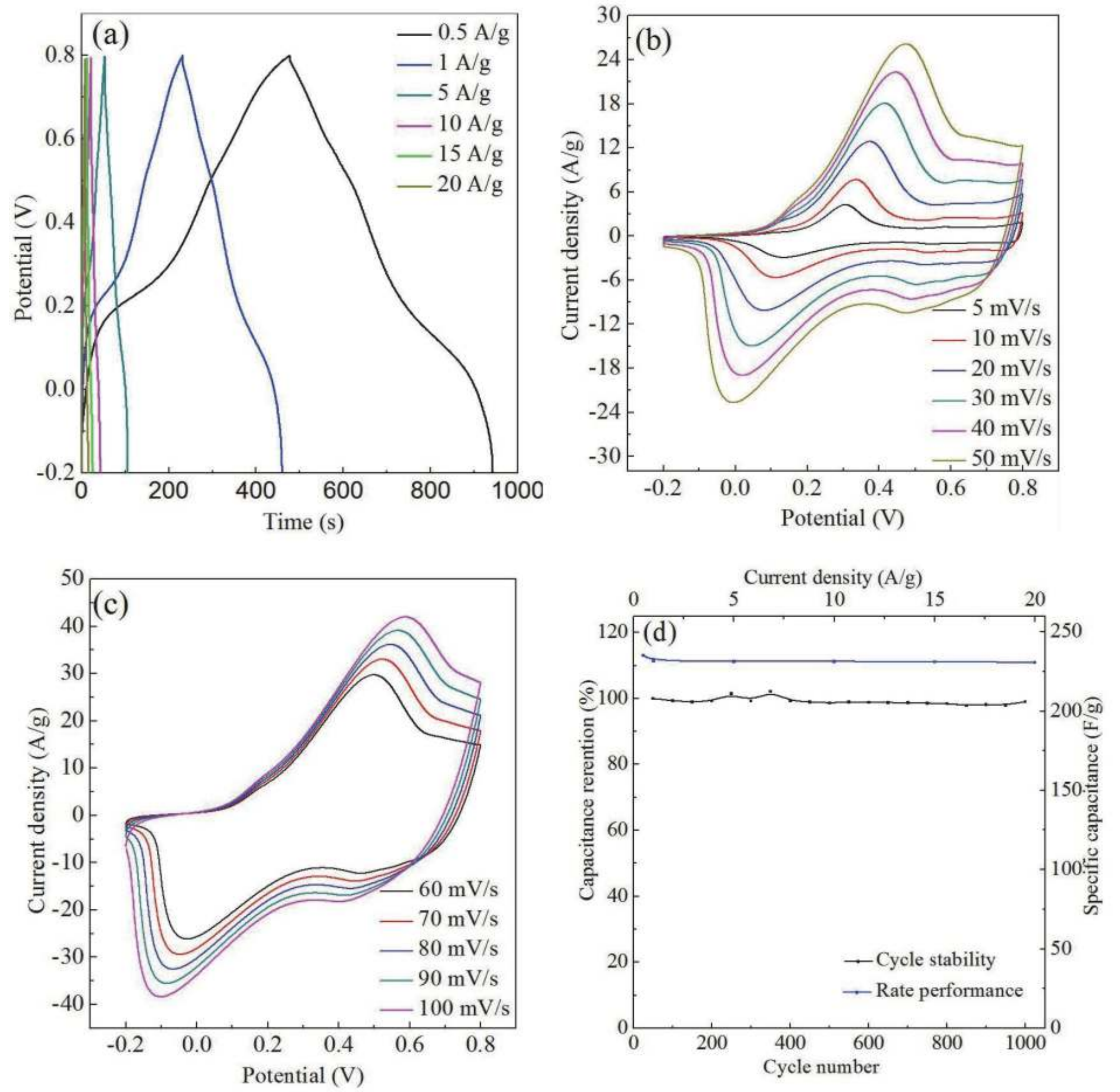

Fig. 5. (Color online) (a) GCD curves of CF|PANI3 composite electrode at different current densities. (b) CV curves for the CF|PANI3 composite electrode at low scan rates. (c) CV curves for the CF|PANI3 composite electrode at high scan rates. (d) Cyclic stability and rate performance of the CF|PANI3 composite electrode.

electrode (97.98 F/g). As the scan period further increases, the corresponding specific capacitance begins to decrease (153.65 F/g for CF|PANI4 electrode and only 70.21 F/g for CF|PANI5 electrode). This result once again proves that proper deposition cycle has an important influence on the capacitance performance of the CF|PANI electrode. This is due to the moderate amount loading of PNAI, which helps to avoid stacking and gets a better layered structure. Furthermore, the U_{drop} of above electrodes also increases as the deposition cycle increases. This happens because the long electrodeposition cycle which can affect the conductivity of the CF|PANI electrodes.

Fig. 5(a) shows curves of the constant current charge and discharge for the CF|PANI3 composite electrode at different current densities. As the current density increases, the charge and discharge time of the CF|PANI electrodes begin to decrease, and the corresponding voltage drop also increase. The calculation of the specific capacitance shows that the CF|PANI3 composite electrode has a large specific capacitance at a lower current density. This happens because the diffusion of electrolyte ions is insufficient at higher current density, resulting in a decrease in specific capacitance[42]. Figs. 5(b) and 5(c) show CV curves of the CF|PANI3 at different scan rates. It can be detected that the directions of cathodic and anodic peaks of the CF|PANI3 electrode are gradually and regularly shifting to the negative and positive orientations as the scan rate increases[42]. Also, the directions of the cathodic and anodic peaks shift to more negative and positive orientations with the higher scan rates, which is due to the fact that ions in the electrolyte are not sufficiently diffused onto the electrode material at higher scan rates, resulting in a loss of effective specific capacitance. Moreover, the

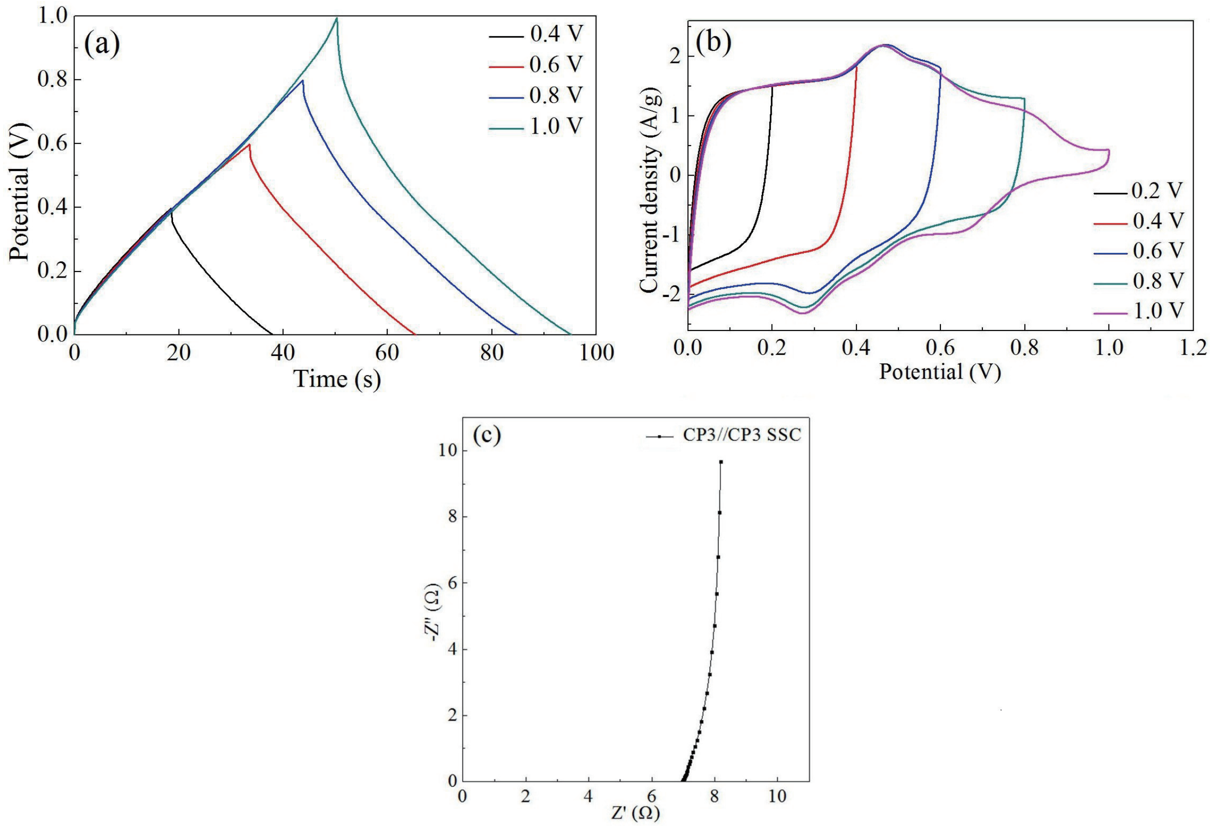

Fig. 6. (Color online) (a) GCD curves of the CP3//CP3 SSC. (b) CV curves of the CP3//CP3 SSC at different voltage windows. (c) EIS of the CP3//CP3 SSC.

low internal resistance of the CF|PANI3 electrode contributes to rapid electron transfer and transfer, which greatly improves its rate performance[43]. Fig. 5(d) shows the little change of the specific capacitance for the CF|PANI3 electrode and 98.15% capacity retention from 0.5 A/g (235.12 F/g) to 20 A/g (230.77 F/g). This result indicates that the CF|PANI3 electrode possesses excellent rate performance. In addition, the CF|PANI3 electrode exhibits a capacity retention rate of 99.04% after 1000 cycles. This is mainly due to the excellent conductivity of the CF substrate, and the pre-treated active sites adhere well to the PANI nanomaterials electrodeposited thereon.

Fig. 6(a) shows the GCD of the CP3//CP3 SSC with different voltage windows at 3 A/g, and Fig. 6(b) shows the CV diagram of the CP3//CP3 SSC at a sweep speed of 20 mV/s. From Figs. 6(a) and 6(b), the electric double layer energy storage characteristics of the CP3//CP3 SSC are exhibited with voltage windows at 0.2 and 0.4 V, but there is almost no redox peak for the CP3//CP3 SSC at the lower operating voltage window. The redox peak begins to appear and pseudo-capacitance characteristics also gradually show up for the CP3//CP3 SSC until the voltage window increases to 0.6 V[44]. However, the capacitance of the CP3//CP3 SSC is not very large due to the limitations of the voltage window. Fig. 6(c) shows the impedance spectrum of the CP3//CP3 SSC from 0.01 to 100 000 Hz, which includes the internal resistance (R_s) and the charge transfer resistance (R_{ct}). In the high frequency region, the line intersects the real axis at a point and the corresponding Rs of the CP3//CP3 SSC is about 6.98 Ω. From Fig. 6(c), the as-prepared CP3//CP3 SSC displays little R_s and R_{ct} due to good conductivity of the CF|PANI3 electrode. Moreover, the CP3//CP3 SSC with a very vertical line at low frequency. This happens because the CF|PANI3 electrode has good electron and ion transport channels, and the pore size distribution makes the electrolyte easily penetrate into the pores[45]. This is attributed to the synergistic effect of the high conductivity and excellent catalytic activity of the CF and the nano PANI.

Table 2 shows the calculation results of the capacitance performance parameters of the CP3//CP3 SSC at different current densities. At a current density of 0.5 A/g, the U_{drop} is less than 0.01 V, while at 20 A/g, the U_{drop} achieves 0.35 V. The corresponding specific capacitance retention rate of the CP3//CP3 SSC is up to 98.15%. This is attributed to the small internal resistance for the CF|PANI3 electrode without adhesives. Simultaneously, the PANI with nanoscale structure covered on the CF surface provides more excellent conductivity, which contributes to the good performance of the pseudo-capacitance for the CP3//CP3 SSC. The specific capacitance C_t of the CP3//CP3 SSC with the CF|PANI3 electrodes is only 1/4 times than that of the single electrode specific capacitance C_s (ie, C_t = C_s/4)[46]. Moreover, the corresponding energy density of the CP3//CP3 SSC decreases as the power density increases. This means that a supercapacitor with high power density is difficult to own a large energy density.

To further improve the situation of the energy density and power density, an asymmetric hybrid supercapacitor was prepared and researched. Figs. 7(a) and 7(c) show the GCD and CV plots of the MM//CP3 ASC with different voltage windows. From Figs. 7(a) and 7(c), it can be seen that the slope of the GCD curves for the MM//CP3 ASC begins to decrease as the voltage increases. In addition, the redox peak in the CV

Table 2. Capacitance performance parameters of the CP3//CP3 SSC at different current densities.

J (A/g)	0.5	1	5	10	15	20
U_{drop} (V)	0.009	0.02	0.097	0.183	0.273	0.35
Δt (s)	466.1	227	41.8	18.9	11.2	7.5
C_s (F/g)	235.12	231.63	231.45	231.33	231.09	230.77
C_t (F/g)	58.78	57.91	57.83	57.83	57.77	57.69
E (W·h/kg)	8.02	7.72	6.55	5.36	4.24	3.39
P (W/kg)	61.93	122.49	564.37	1021.23	1363.15	1625.01

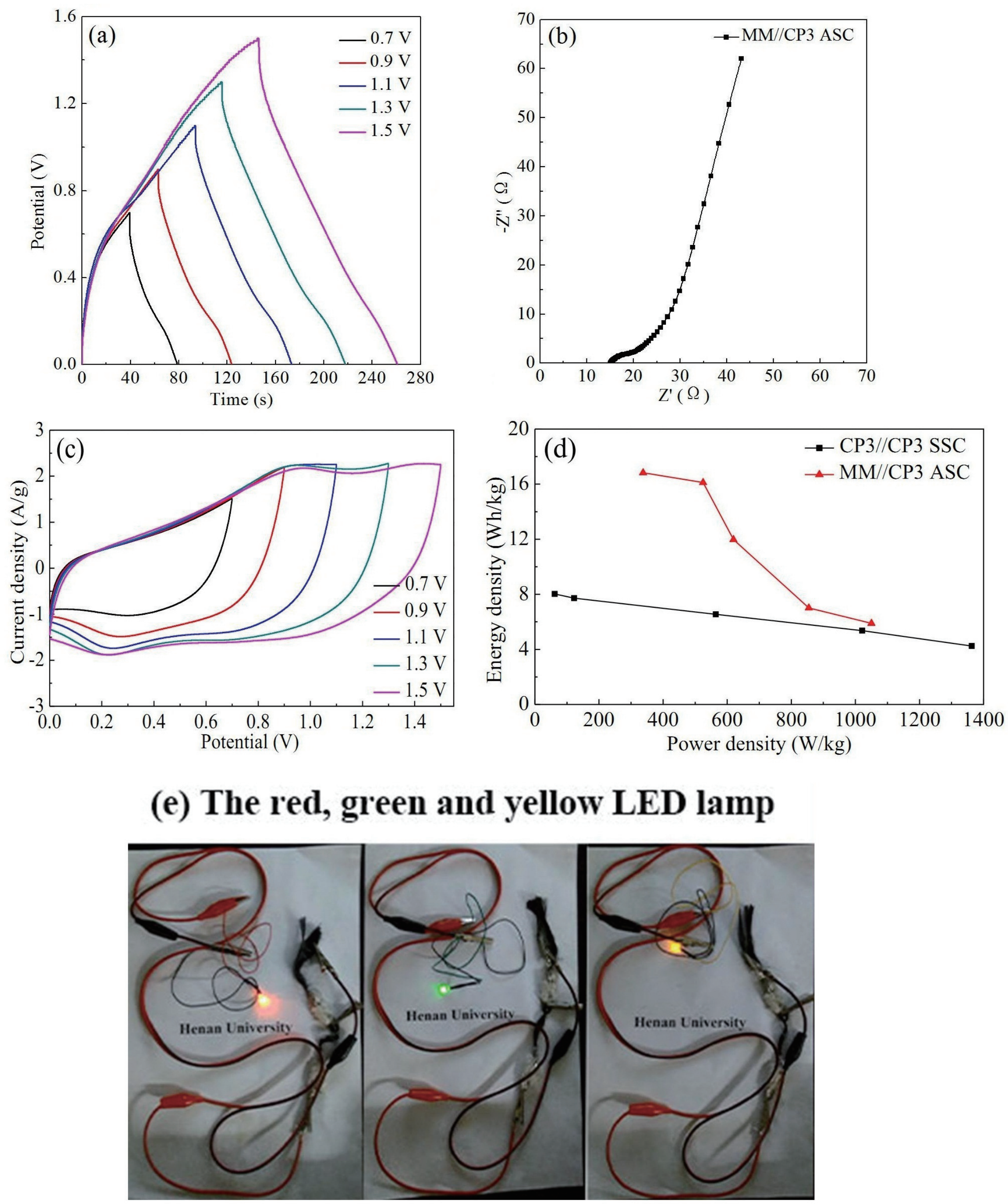

Fig. 7. (Color online) (a) GCD of the MM//CP3 ASC under different voltage windows. (b) EIS of the MM//CP3 ASC. (c) CV curves of the MM//CP3 ASC under different voltage windows. (d) Relationships between the energy density and power density of the CP3//CP3 SSC and MM//CP3 ASC. (e) The red, green and yellow LED lamps are lit by two series MM//CP3 ASC.

curves gradually appears as the scan voltage increases. This result indicates that a larger voltage window contributes to the performance of the tantalum capacitor. At the same time, it is known from the Eq. (3) that a larger operating voltage is also beneficial to the improvement of the energy density of the supercapacitor. Usually, the specific capacitance of the MM//CP3 ASC can reach 59.2 F/g at a current density of 0.75 A/g (current density through CF|PANI3 electrode is 1.16 A/g), which is slightly higher than that of the CP3//CP3 SSC. However, the energy density of the MM//CP3 ASC is greatly improved as the operating voltage window increases to above 1 V. Furthermore, the energy density of the MM//CP3 ASC can reach 16.12 W·h/kg, which is significantly higher than that of the CP3//CP3 SSC at a power density of 525.03 W/kg. Fig. 7(b) shows the EIS of the MM//CP3 ASC. This displays that the solution internal resistance R_s is 15 Ω, and its charge transfer internal resistance R_{ct} is about 8 Ω. In addition, the slope of the line is large in the low frequency region, indicating good capacitive response characteristics and ion-clearing channels[45]. Therefore, the overall R_s of the quasi-solid MM//CP3 ACS is greater than that of the simple superposition of positive and negative resistances, which has a close relationship with the matching degree of positive and negative materials. Fig. 7(d) presents the relationships between the energy density and power density of the CP3//CP3 SSC and MM//CP3 ASC. The energy density of the MM//CP3 ASC decreases seriously with the increasing power density. This happens because the matching degree between positive and negative materials is distinguished under different power densities. Therefore, a power supply equipment suitable for rated power of electrical appliances can be prepared by adjusting the charge balance of positive and negative electrodes under a specific power density. In general, the contribution of asymmetric supercapacitors in voltage window and energy density is still significant. Fig. 7(e) shows that red, green and yellow LED bulbs can easily be lit by two series MM//CP3 ASCs, which shows a good potential application.

4. Summary

PANI nanoparticles were in situ coated onto the surface of the electrochemically activated CF by using electrochemical deposition method. In the absence of adhesive, the low internal resistance of the CF substrate can not only help to reduce the voltage drop to maintain a large voltage window but the PANI nanoparticles also have a better pseudo-capacitance to improve the specific capacity of the CF|PANI3 composite electrode. The CF|PANI3 electrode still has a 99.6% retention when the current density increases from 1 to 20 A/g, showing good rate performance and excellent cycle stability. This happens because the nanoscale PANI which can be deposited on the pretreated CF surface controllably and efficiently without binder by using the electrodeposition method. In addition, the prepared MM//CP3 ASC has higher energy density than that of the CP3//CP3 SSC. This is attributed to the expansion of operating voltage window, which helps to improve its energy density. Two MM//CP3 ASCs after being connected in series can easily light a red, green or yellow LED lamp. These results indicate that the neutral quasi-solid MM//CP3 ASC has a good application prospect.

Acknowledgements

The authors are very grateful to the joint support by NSFC (No. 61704047).

References

[1] Amaral M M, Venâncio R, Peterlevitz A C, et al. Recent advances on quasi-solid-state electrolytes for supercapacitors. J Energ Chem, 2022, 67, 697
[2] Liu T C, Sutarsis S, Zhong X Y, et al. An interfacial wetting water based hydrogel electrolyte for high-voltage flexible quasi solid-state supercapacitors. Energy Storage Mater, 2021, 38, 489
[3] Wang P, Zhang Y, Jiang H, et al. Ammonium vanadium oxide framework with stable NH_4^+ aqueous storage for flexible quasi-solid-state supercapacitor. Chem Eng J, 2022, 427, 131548
[4] Gu P, Liu W, Hou Q, et al. Lignocellulose-derived hydrogel/aerogel-based flexible quasi-solid-state supercapacitors with high-performance: a review. J Mater Chem A, 2021, 9, 14233
[5] Fagiolari L, Sampò M, Lamberti A, et al. Integrated energy conversion and storage devices: Interfacing solar cells, batteries and supercapacitors. Energy Storage Mater, 2022, 51, 400
[6] Cherusseri J, Pandey D, Kumar K S, et al. Flexible supercapacitor electrodes using metal–organic frameworks. Nanoscale, 2020, 12, 17649
[7] Su S, Lai L, Li R, et al. Annealing-assisted dip-coating synthesis of ultrafine Fe_3O_4 nanoparticles/graphene on carbon cloth for flexible quasi-solid-state symmetric supercapacitors. ACS Appl Energy Mater, 2020, 3, 9379
[8] Chen Q, Miao X, Liu Y, et al. Polyaniline electropolymerized within template of vertically ordered polyvinyl alcohol as electrodes of flexible supercapacitors with long cycle life. Electrochim Acta, 2021, 390, 138819
[9] Lee K S, Jeong H T. Development and optimization of ionic liquid based gel polymer electrolyte for all solid-state supercapacitor. J Energy Storage, 2021, 42, 103001
[10] Du P, Dong Y, Dong Y, et al. Fabrication of uniform MnO_2 layer-modified activated carbon cloth for high-performance flexible quasi-solid-state asymmetric supercapacitor. J Mater Sci, 2022, 57, 3497
[11] Wang W, Xu H, Zhao W, et al. Porphyrin-assisted synthesis of hierarchical flower-like polypyrrole arrays based flexible electrode with high areal capacitance. Chem Eng J, 2022, 428, 131089
[12] Quan B, Meng Y, Li L, et al. Vertical few-layer graphene/metalized Si-nanocone arrays as 3D electrodes for solid-state supercapacitors with large areal capacitance and superior rate capability. Appl Surf Sci, 2017, 404, 238
[13] Wang K, Zheng B, Mackinder M, et al. Efficient electrophoretic deposition of MXene/reduced graphene oxide flexible electrodes for all-solid-state supercapacitors. J Energy Storage, 2021, 33, 102070
[14] Zang L, Qiao X, Liu Q, et al. High-performance solid-state supercapacitors with designable patterns based on used newspaper. Cellulose, 2020, 27, 1033
[15] Wang Y, Chu X, Zhu Z, et al. Dynamically evolving 2D supramolecular polyaniline nanosheets for long-stability flexible supercapacitors. Chem Eng J, 2021, 423, 130203
[16] Huang Z, Li L, Wang Y, et al. Polyaniline/graphene nanocomposites towards high-performance supercapacitors: A review. Comp Comm, 2018, 8, 83
[17] Chu X, Zhao X, Zhou Y, et al. An ultrathin robust polymer membrane for wearable solid-state electrochemical energy storage. Nano Energy, 2020, 76, 105179
[18] Heme H N, Alif M S N, Rahat S M S M, et al. Recent progress in polyaniline composites for high capacity energy storage: A review. J Energy Storage, 2021, 42, 103018
[19] Chang X, El-Kady M F, Huang A, et al. 3D graphene network with covalently grafted aniline tetramer for ultralong-life supercapacitors. Adv Funct Mater, 2021, 31, 2102397
[20] Wei Y, Zheng M, Luo W, et al. All pseudocapacitive MXene-MnO_2 flexible asymmetric supercapacitor. J Energy Storage, 2022, 45, 103715
[21] Zhu Y, Wang D, Yan X, et al. Vertical, dense and uniform V_2O_5 nanoneedle arrays on carbon foam for boosting electrochemical per-

formance. J Energy Storage, 2021, 37, 102492
[22] Sekhar S C, Nagaraju G, Ramulu B, et al. An eco-friendly hot-water therapy towards ternary layered double hydroxides laminated flexible fabrics for wearable supercapatteries. Nano Energy, 2020, 76, 105016
[23] Hong X, Wang X, Li Y, et al. Potassium citrate-derived carbon nanosheets/carbon nanotubes/polyaniline ternary composite for supercapacitor electrodes. Electrochim Acta, 2022, 403, 139571
[24] Wang X, Wang Y, Liu D, et al. Opening MXene ion transport channels by intercalating PANI nanoparticles from the self-assembly approach for high volumetric and areal energy density supercapacitors. ACS Appl Mater Interfaces, 2021, 13, 30633
[25] Iqbal M Z, Faisal M M, Ali S R, et al. Co-MOF/polyaniline-based electrode material for high performance supercapattery devices. Electrochim Acta, 2020, 346, 136039
[26] Majumder M, K. Thakur A, Bhushan M, et al. Polyaniline integration and interrogation on carbon nano-onions empowered supercapacitors. Electrochim Acta, 2021, 370, 137659
[27] Xu M, Guo H, Zhang T, et al. High-performance zeolitic imidazolate frameworks derived three-dimensional Co_3S_4/polyaniline nanocomposite for supercapacitors. J Energy Storage, 2021, 35, 102303
[28] Chen W, Jiang S, Xiao H, et al. Graphene modified polyaniline-hydrogel based stretchable supercapacitor with high capacitance and excellent stretching stability. ChemSusChem, 2021, 14, 938
[29] Cheng B, Cheng R, Tan F, et al. Highly efficient quasi-solid-state asymmetric supercapacitors based on MoS_2/MWCNT and PANI/MWCNT composite electrodes. Nanoscale Res Lett, 2019, 14, 66
[30] Hsu C, Hu C, Wu T, et al. How the electrochemical reversibility of a battery-type material affects the charge balance and performances of asymmetric supercapacitors. Electrochim Acta, 2014, 146, 759
[31] Singh R, Tripathi C C. Study of graphene based flexible supercapacitors with different gel electrolytes. Mater Today Proc, 2018, 5, 943
[32] Grote F, Zhao H, Lei Y. Self-supported carbon coated TiN nanotube arrays: innovative carbon coating leads to an improved cycling ability for supercapacitor applications. J Mater Chem A, 2015, 3, 3465
[33] Guo T, Zhou D, Liu W, et al. Recent advances in all-in-one flexible supercapacitors. Sci China Mater, 2021, 64, 27
[34] Yan J, Fan Z, Sun W, et al. Advanced asymmetric supercapacitors based on $Ni(OH)_2$/Graphene and porous graphene electrodes with high energy density. Adv Funct Mater, 2012, 22, 2632
[35] Gao Y, Huang K, Wu X, et al. MoS_2 nanosheets assembling three-dimensional nanospheres for enhanced-performance supercapacitor. J Alloys Compd, 2018, 741, 174
[36] Li H, Liang J, Li H, et al. Activated carbon fibers with manganese dioxide coating for flexible fiber supercapacitors with high capacitive performance. J Energ Chem, 2019, 31, 95
[37] Nam M S, Patil U, Park B, et al. A binder free synthesis of 1D PANI and 2D MoS_2 nanostructured hybrid composite electrodes by the electrophoretic deposition (EPD) method for supercapacitor application. RSC Adv, 2016, 6, 101592
[38] Meng Y, Gu D, Zhang F, et al. A family of highly ordered mesoporous polymer resin and carbon structures from organic-organic self-assembly. Chem Mater, 2006, 18, 4447
[39] Ren L, Zhang G, Yan Z, et al. Three-dimensional tubular MoS_2/PANI hybrid electrode for high rate performance supercapacitor. ACS Appl Mater Interfaces, 2015, 7, 28294
[40] Lu X, Hu Y, Wang L, et al. Macroporous carbon/nitrogen-doped carbon nanotubes/polyaniline nanocomposites and their application in supercapacitors. Electrochim Acta, 2016, 189, 158
[41] Luo Y, Zhang H, Guo D, et al. Porous $NiCo_2O_4$-reduced graphene oxide (rGO) composite with superior capacitance retention for supercapacitors. Electrochim Acta, 2014, 132, 332
[42] Chen Y, Xu B, Wen J, et al. Design of novel wearable, stretchable, and waterproof cable-type supercapacitors based on high-performance nickel cobalt sulfide-coated etching-annealed yarn electrodes. Small, 2018, 14, 1704373
[43] Liu T, Zhang F, Song Y, et al. Revitalizing carbon supercapacitor electrodes with hierarchical porous structures. J Mater Chem A, 2017, 5, 17705
[44] Choudhary N, Li C, Moore J, et al. Asymmetric supercapacitor electrodes and devices. Adv Mater, 2017, 29, 1605336
[45] Wang J, Zhang Y, Ye J, et al. Facile synthesis of three-dimensional $NiCo_2O_4$ with different morphology for supercapacitors. RSC Adv, 2016, 6, 70077
[46] Zhang Z, Wang G, Li Y, et al. A new type of ordered mesoporous carbon/polyaniline composites prepared by a two-step nanocasting method for high performance supercapacitor applications. J Mater Chem A, 2014, 2, 16715

Kexin Li received her BS degree in 2021 after graduating from Zhengzhou Normal University. Now she is a master's student at Henan University. Since September 2021, she has been working in Prof. Furui Tan's research group under the supervision of Associate Professor Gentian Yue. Her current research focuses on supercapacitors.

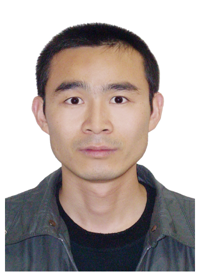

Gentian Yue received his Ph.D. degree from Huaqiao University, China in 2013. Since then, he has been working as a full time associate professor at Henan Key Laboratory of Photo voltaic Materials, Henan University, China. His research interests include material synthesis and device fabrication of dye sensitized solar cells, supercapacitor, and energy capture and storage devices for wearable electronics.

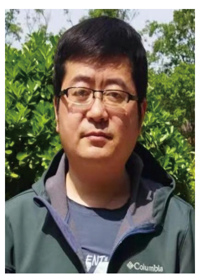

Furui Tan is currently a professor in the Henan Key Laboratory of Photovoltaic Materials, Henan University, China. He received his Ph.D. degree from Institute of Semiconductors, Chinese Academy of Sciences (ISCAS) in 2011. He joined the Sargent group in the Department of Electronics and Computer Engineering (ECE) in the University of Toronto, as a visiting scholar in 2017.6 and 2018.6. His research group focuses on organic and nanoscale materials for solar cells, photodetectors, and electrocatalysis, etc.